agronomy

MDPI

Article

The Method and Experiment of Kinetic Determination for the Rotary Soil-Engaging Components of Agricultural Machinery Using a Compacting Device in a Paddy Field as an Example

Jinwu Wang , Yushun Xiang, Changyu Wang, Changsu Xu, Guixuan Zhu, Zejun Gu, Jinfeng Wang and Han Tang *

College of Engineering, Northeast Agricultural University, Harbin 150030, China
* Correspondence: tanghan@neau.edu.cn; Tel.: +86-18746074120

Abstract: In order to explore the influence of soil force on rotary soil-engaging components during their operation, a kinetic parameter measurement system of rotary soil-engaging components was developed via the sensor strain measurement technique. By taking a single-sided compacting ridge device as an example, the kinetic experiment was carried out on the operation parameters of the compacting device and obtained the variation law of the force of the soil on the pinnae. ADAMS software was used to simulate the operation of the compacting device under different experimental factors (soil moisture content, forward speed of the ridge device, and the rotation speed of the compacting device), and the test data were obtained; the experiment was carried out with the forward speed of the soil tanker and the rotation speed of the compacting device as the experimental factors, and the average of the force of soil on the pinnae and the firmness value of the ridge were the experimental indicators. The results showed that under a moisture content of 27%, the forward speed of the device was 0.8 km·h^{-1}, the maximum firmness of the ridge was 1233.21 kPa, the minimum firmness of the ridge was 953.85 kPa, and the coefficient of variation of the stability of the firmness value of the ridge was 8.04; the force of the pinnae on the soil increased with an increase in the forward speed of the soil tanker, and the variation range of the force was 2838.1–5695.2 N. It was verified that the design of this operation parameter measurement system for rotary soil-engaging components meets the practical requirements and also provides an important reference for the measurement of the relevant parameters of similar rotary soil-engaging components.

Keywords: rotary soil engaging; compacting device; kinetic measurement; experiment

check for updates

Citation: Wang, J.; Xiang, Y.; Wang, C.; Xu, C.; Zhu, G.; Gu, Z.; Wang, J.; Tang, H. The Method and Experiment of Kinetic Determination for the Rotary Soil-Engaging Components of Agricultural Machinery Using a Compacting Device in a Paddy Field as an Example. *Agronomy* **2023**, *13*, 775. https://doi.org/10.3390/agronomy13030775

Academic Editor: Dionisio Andújar

Received: 15 February 2023
Revised: 5 March 2023
Accepted: 6 March 2023
Published: 7 March 2023

1. Introduction

Rotary soil-engaging components are mainly used in agricultural machinery to compact the soil so that the soil can obtain the appropriate soil bulk density, and the behavior law of the machinery acting on the soil and the soil in response to machinery can be explored. At present, domestic and foreign scholars have carried out a lot of research on the compaction characteristics of the soil after the rotary soil-engaging components contact the soil. Liu et al. [1] designed the cylindrical belt suppressor with variable pressure and realized the real-time monitoring of the compaction pressure during the sowing operation, but its complex structure increased the difficulty in the processing process. Matin et al. [2,3] optimized the commonly used rotary tillage blades for disturbance soil cultivation design and, through bench testing, verified the accuracy of their conclusions, which has improved the efficiency of strip cultivation. Mustafa et al. [4–6] tested wheel loaders using the discrete element method and verified the reliability of using DEM simulation to study the movement processes of soil and tools. Wang et al. [7] designed a bionic press roller for the soil adhesion phenomenon during the operation of rotary soil-engaging components, but the processing cost of this press roller is high, the soil compactness after compaction is uneven, and the rolling resistance is large. Ma et al. [8] conducted experimental studies on the interaction between rotary soil-engaging components and soil, and the results showed that the mechanical properties of the rotary soil-engaging components were affected by the contact stress of the interface and the lower soil stress. Zhang et al. and Salem et al. [9,10] used the finite element method to establish a two-dimensional model of rotary soil-engaging components: soil (and applied pressure to the rotary soil-engaging components according to the mechanical properties), initial bulk density, and the moisture content of the soil and calculated the compactness of the soil; however, due to the relative friction generated between the rotary soil-engaging components and the soil during operation, it is difficult to measure the kinetic parameters of the rotary soil-engaging components themselves, so there are few reports in the literature regarding the determination of the kinetic parameters of the rotary soil-engaging components during operation.

Paddy field ridging has a typical rotary soil-engaging component; the ridge of a paddy field belongs to the tillage and preparation in the process of rice production; at present, domestic field construction is still based on manual labor, and its construction quality is poor, the operation cycle is long, and the repetitive labor intensity is high. Solid and reasonable fields are an important guarantee for flooded irrigation and rice production, which can increase the yield of food crops, reduce water waste, and help the construction of standardized farmland [11,12], which is of great significance to the safe development of food production [13]. The mechanized ridging of paddy fields is a technology that meets the requirements of rice irrigation and production by using agricultural machinery. From the 1960s, domestic and foreign scholars began to study paddy field ridge technology and its related machinery [14–16], of which Japan's research on this technology is relatively mature. Japan's research combined electromechanical and hydraulic technologies for design, which can automatically adjust the direction of the components of the ridge and improve the firmness and stability of the ridge. However, its price is high, the maintenance is inconvenient, and the soil quality of the paddy fields in Japan and China is quite different, so it is not suitable for large-scale promotion and use in various regions in China [17,18]. In order to improve the quality and efficiency of paddy field ridging, Wang et al. [19] researched and designed the 1DSZ-350 type hanging unilateral rotary tillage compacting ridge for paddy fields, which provided theoretical support and a technical reference for the innovative research and development and optimization of paddy field mechanized construction machinery. Since then, some domestic scientific research institutes and agricultural machinery enterprises have also successively studied and designed paddy field ridges, mainly via a split plow or rotary tiller and other components to take soil on both sides and two-sided disc rolling to compact the ridge [14,20,21].

By taking the single-side compacting ridge device as an example, this paper combines the structure, operating parameters, and soil conditions of the rotary soil-engaging components to design a kinetic measurement system for the operating parameters of rotary soil-engaging components. This paper takes the compacting device as the research object, measuring its related kinetic parameters, obtaining the variation law of the force of the soil on the pinnae, and establishing a mathematical model of the correlation, which can explore the relationship between the force of the soil on the pinnae, the firmness of the field ridge, and the operating parameters of the compacting device. The aim is to obtain (through experiments) the variation laws of the acting force of soil on the blades and the firmness of the constructed ridges with changes in the forward speed of the implement and the rotational speed of the compaction device, providing a theoretical basis for the optimization of the compaction device and the structural design of the whole machine. Testing the applicability of the design system can provide an experimental basis for the whole machine design, solve the related kinetics, and provide a method for the measurement of the kinetic parameters of rotary soil-engaging components.

2. Materials and Methods

2.1. The Overall Structure and Operation Principle of Compacting Device

The compacting device of a paddy field is mainly composed of superimposed elastic pinnae, compacting rollers, and various connecting components. Each elastic pinna has a bent, fan-shaped structure, which is bent into two sections, and 10 elastic pinnae of the same size and shape are evenly superimposed and distributed in the form of steps to form a conical table-shaped pinnae combination (Figure 1).

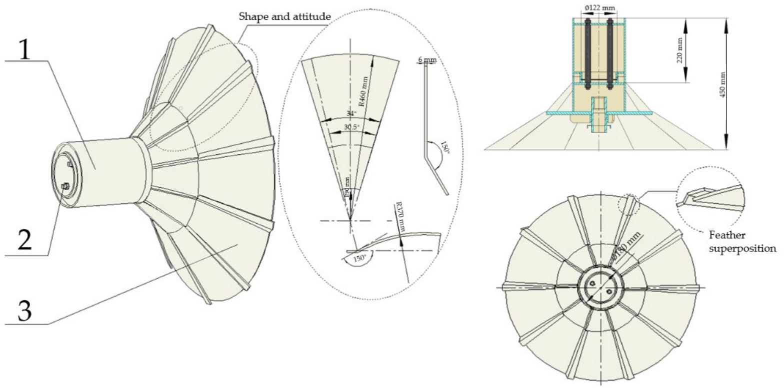

Figure 1. Schematic diagram of the structure of the compacting device. 1. Compacting rollers; 2. Connecting shaft; 3. Superimposed elastic pinnae.

During the operation, the compacting device advances and rotates forward in the direction of the operation of the driving machinery, and the rotation speed is faster than the forward speed of the driving machinery. The rotation of the compacting roller of the compacting device pushes the soil gathered by the rotary cutting components of the soil collection and the retaining shell cover to the top, shoulder, and side of the ridge. As the superimposed elastic pinnae rotate and squeeze the soil, the elastic pinnae create an elastic deformation, produces certain vibrations, repeatedly pats the soil, and continuously reduces the gap between the soil particles, forming the ridge (Figure 2).

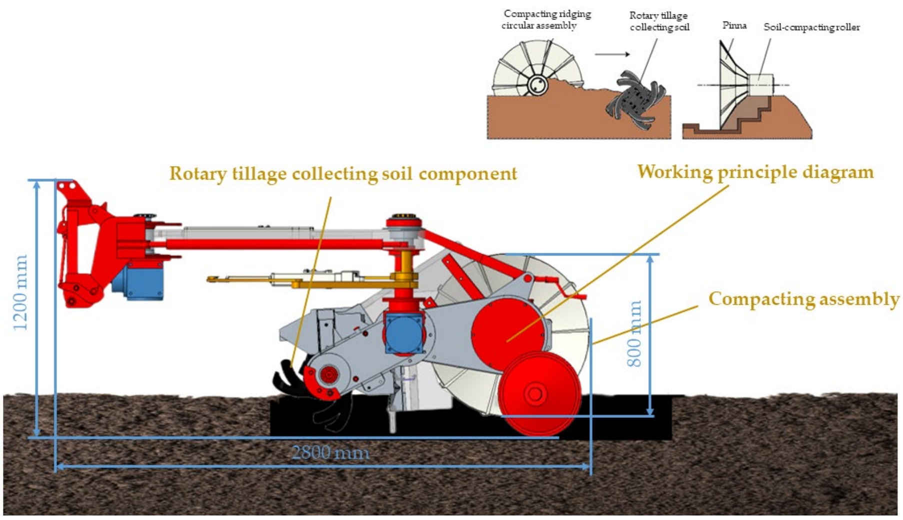

Figure 2. Schematic diagram of ridge device of a paddy field.

2.2. Design of Kinetic Test System

The compaction device of the ridge builder compacts the ridges to a certain degree of firmness. To obtain the force of the blades on the soil during the operation of the compaction device, a dynamic testing platform for the compaction and ridge-building device was established, effectively avoiding excessive wear of the blades due to long-term contact with the soil during the ridge-building process, and studying the vibration dynamic characteristics parameters of the whole machine. By using the resistance-strain gauge sensing principle, a dynamic testing system for working out the parameters was constructed, with the forward speed of the implement and the rotational speed of the compaction and ridge-building device as the experimental factors, and the average force of the soil on the blades and the firmness of the ridges as the experimental indicators to determine the force of the soil on the blades during the compaction and ridge-building process.

In order to explore the force of the pinnae during the action of the compacting device of the ridge and the soil and measure the related parameters, a kinetic test system for the operation parameters of the compacting device was built, and the pinnae of the strain gauge were pasted onto the compacting device, connected to the kinetic operation parameter test system, and collected in real-time.

In order to obtain high test sensitivity, a full-bridge test circuit was used to measure the force of the soil on the pinnae. In the actual process of the operation, it is difficult to paste the test strain gauge on the side where the compacting device is in direct contact with the soil during the kinetic test because the outer rotation of the compacting device contacts the soil, and the soil exerts certain friction on the compacting device. According to material mechanics, the pinnae is composed of many longitudinal fibers which are parallel to the axial curve, which will inevitably cause the fibers near the inside of the pinnae to be elongated and the fibers near the outside of the pinnae to be shortened when bending deformation occurs, and the corresponding elongation is equal to the shortening amount. In order to create stability in this test, the strain gauge was selected to paste onto the side of the inner wall of the compacting device away from the soil, forming a Wheatstone full-bridge circuit, and the variation of the force of the soil on the pinnae was obtained from the induced voltage variation. When the compacting device was subjected to the force of the soil (when operating and a slight deformation of the elastic pinnae occurs), the sensor group of the strain gauge transmits the variable voltage signal to the collector ring (to prevent entanglement of wires), transmits the signal to the data acquisition instrument through the collector ring, transmits the signal to the computer by regulating the strain, and then uses the DASP-10 software for the computer to obtain the corresponding strain curve and processes it (Figure 3).

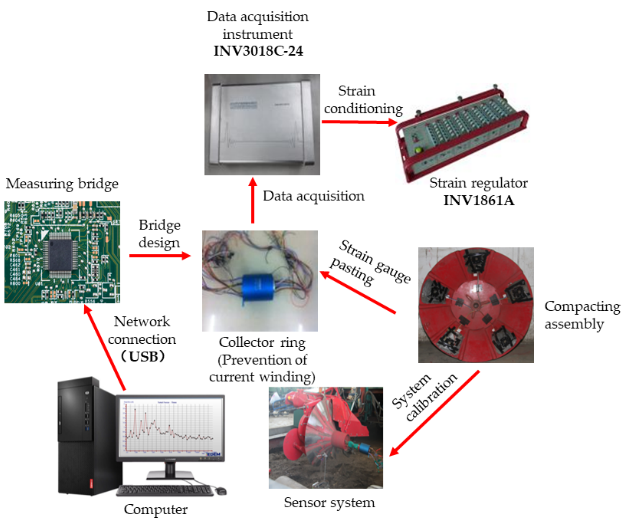

Figure 3. Flow chart of the test system of the operating parameter.

2.3. Simulation Analysis of the Operation of the Compacting Device

As one of the key components of ridge machinery of paddy fields, the operation performance of the compacting device directly affects the shape of the soil after the deformation of the force and determines the firmness of the ridge soil, which is related to the water storage ability of the ridge, which then affects the growth of the crops of the paddy field; therefore, it is very necessary to research the interaction between soil and compacting device in operation. Through preliminary experiments, it was found that the properties of the soil with different moisture content varied greatly, and the effect of the compaction on the ridge was obvious. According to the soil state of paddy fields in Northeast China, the combination of kinetic parameters and optimal operation parameters of the ridge forming of the compacting device under different conditions was determined by combining it with the finite element simulation method [22–25].

2.3.1. Finite Element Model of Suppression Device for Soil

The soil moisture content required for ridging the paddy field was between 24–30% during the period of the ridging [26], and three plots with different moisture contents (24%, 27%, and 30%) were rotated in the preliminary experiments; the related soil parameters were obtained in combination with the literature, and the specific parameters are shown in Table 1.

Table 1. Finite element model of soil parameters.

Parameters	Value		
	Soil Moisture Content		
	24%	27%	30%
Soil density/kg·m^{-3}	1255	1480	1550
Elastic modulus/MPa	1.32	1.41	1.65
Poisson's ratio	0.38	0.38	0.38
Cohesion/kPa	10.12	10.57	12.35
Friction angle/°	16.25	16.81	17.73

The ideal single-sided soil section is shown in Figure 4b. The height of the ridge is 355 mm, the top width of the single side of the ridge is 172 mm, the bottom width of the single side of the ridge is 422 mm, the shoulder length of the ridge is 145 mm, the side length of the ridge is 262 mm, and the overall length of the single side of the ridge soil is 2500 mm.

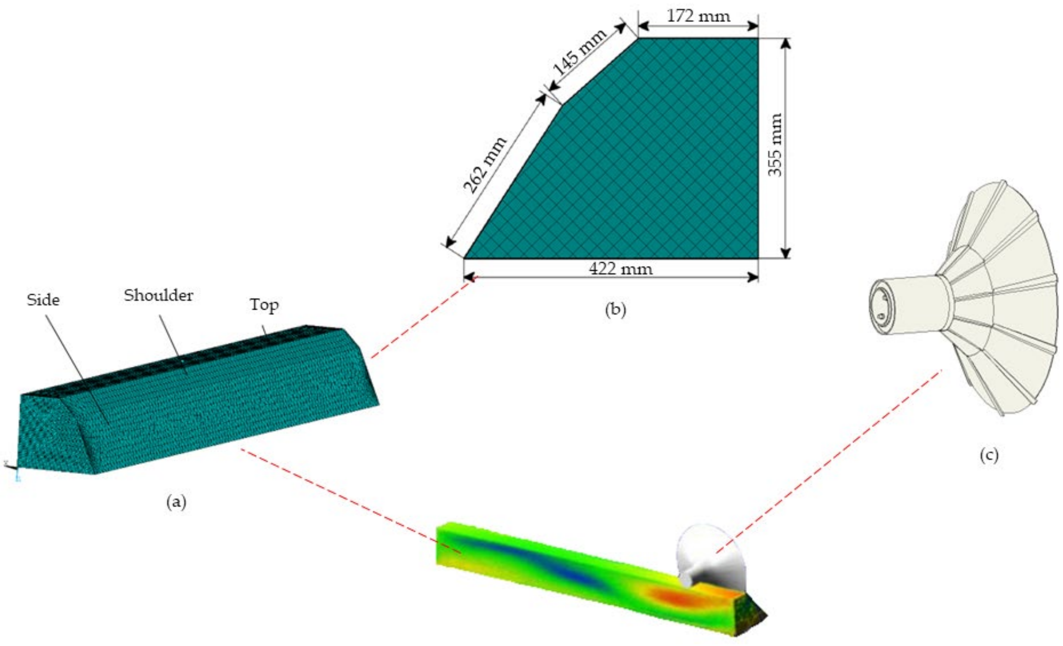

Figure 4. Simulation process and analysis of compacting devices. (**a**) Finite element analysis model of soil mass in field ridge; (**b**) cross-section of soil mass in field ridge; (**c**) three-dimensional diagram of compacting assembly.

(1) Establishment of soil modeling

According to the symmetry of the ridge model, the simplified one-half soil modeling of the ridge is used to shorten the simulation operation time, that is, the single-sided ridge soil model. When taking the soil with a moisture content of 27% as an example, the material is set, and the known parameters, such as elastic modulus, Poisson's ratio, density value, isotropic thermal expansion coefficient value, cohesion, friction angle, and expansion angle, are entered. The cell is added, two key points are established, and the node number and co-ordinate values are entered; the grid is set in the mesh tool of the preprocessor, the four edges are selected in the length direction, and the NDIV is changed to 100, which means that the length direction is 100 equal parts; finally, the volume is selected to generate the mesh. Since the top, shoulder, and side of the established soil model of the ridge are the main parts in contact with the compacting device, the tetrahedral mesh division unit is used to refine the mesh of the contact surface. The total number of grid elements is 120,470, and the total number of nodes is 24,248 (Figure 4a).

2.3.2. Simulation Test Content

In order to explore the influence of the compacting device by the force of the soil during operation, ADAMS software was used to simulate the working situation of the compacting device under different experiment factors (soil moisture content, forward speed of the ridge machinery, and rotation speed of the compacting device), and the corresponding experimental data were obtained; the influence of the above factors on the horizontal operation resistance and the coefficient of variation of the stability of the firmness of the ridge was analyzed by using the Design Export 6.0.10 data analysis software. The forward speed range of the machinery was selected as 0.6–1.0 km·h^{-1}, and the rotation speed range of the compacting device was selected as 300–360 rpm. The total virtual simulation time was set to 10 s, of which the effective operation time was 5 s, and after the simulation test started, the simulation data were kept (saving every 0.01 s to facilitate the subsequent data). The settings of the multifactorial test factor level are shown in Table 2. Under the premise of ensuring that the parameters remain unchanged, each group in the experiment was repeated five times, and the horizontal operation resistance and the coefficient of variation were calculated and recorded after each experiment; finally, the average was selected as the experimental result, and the virtual simulation multifactor orthogonal experiment research was carried out.

Table 2. Experiment factor level coding table.

Level	Factor		
	Soil Moisture Content X_1/%	**Forward Speed X_2/km·h^{-1}**	**Rotation Speed X_3/rpm**
−1	24	0.6	300
0	27	0.8	330
1	30	1.0	360

2.4. Bench Experiment of Kinetic Test

The kinetic test system of the operation parameters of the selfbuilt compacting device is attached to the soil tanker, which can achieve autonomous control. The forward speed of the machinery and the speed of the compacting device are controlled by soil tanker 1; the soil exerts a force on the pinnae and makes recoverable deformation when compacting device 3 operates, and the voltage variation makes the strain gauge sensor group transmit the signal to collector ring 4, the signal is transmitted to strain regulator 5 through the collecting ring, and then the signal is transmitted it to the DASP-10 software of a computer through data collector 6. The analysis of the obtained strain curve can determine the variation of the force, the relationship between the strain variation and the force, and the relationship between the force, the firmness of the ridge, the forward speed of the machinery, and the rotation speed of the compacting device (Figure 5).

The test prototype is a single-sided compacting device, and the test soil in the soil trough bench is cultivated black loam soil from the northeast region (the plant roots, stems, and debris in the soil will not affect the experiment). The absolute moisture content of the soil is (28.2 ± 0.5)%, the average density of the soil is 2610 kg/m^3, and the firmness of the soil is 130–200 kPa by tilling the soil, which is in line with the actual state of operation. During the experiment, the forward speed and the rotation speed of the single-sided ridge device and rotary ridge soil collection cutter roller are controlled by the monitoring auxiliary test bench to realize control via stepless, variable speed; the rotary depth of the tillage can be controlled by the hydraulic suspension mechanism of the test bench; the computer displays signals, such as measured torque and rotation speed, in real-time.

Figure 5. Schematic diagram of the test system for the operating kinetic parameters of the compacting device. 1. Experiment trough tractor of TCC-III computer monitoring-aided test; 2. Three-point suspension; 3. Compacting device; 4. Collecting ring; 5. INV1861A portable strain gauge; 6. INV3018C-24 data collector; 7. Computer.

The stability of the firmness of the ridge is a key factor in ensuring the water storage ability of paddy fields, which directly affects the growth and yield of rice. Therefore, in this experiment, the coefficient of variation of the stability of the firmness of the ridge was selected as the main evaluation index of the quality of the ridge, and the lower the coefficient of variation, the more stable the firmness of the field ridge and the higher the quality of the operation, which can measure the stability of the overall field ridge. An SC900 handheld soil firmness speed tester was used to measure the soil firmness in the field before the operation, and the formula for calculating the coefficient of variation was as follows:

$$Q_i = \frac{\sqrt{\frac{\sum_{i=1}^{n} (q_i - q_0)^2}{n-1}}}{q_0} \times 100\% \tag{1}$$

where n is the number of tests; q_i is the firmness test value of the ridge at the point I, kPa; q_0 is the average of the firmness of the ridge, kPa.

The black soil (different moisture content) in the rice cropping area of Northeast China was used as the calibration test soil, and the model between the firmness of the field ridge and compacting stress under three different moisture content (24%, 27%, and 30%) was established. The specific calibration relationship is:

$$\begin{cases} s_1 = 0.735a_1 + 92.5 & R^2 = 0.9853 \\ s_2 = 0.6425a_2 + 136.75 & R^2 = 0.9835 \\ s_3 = 0.49a_3 + 239 & R^2 = 0.9745 \end{cases} \tag{2}$$

where a_1, a_2, and a_3 are the firmness of the field for manual measurement, s_1, s_2, and s_3 is the uniform compacting stress.

3. Results and Analysis

3.1. Simulation Results of Rotary Soil-Engaging Components

Results and Analysis of Simulation

In the virtual simulation test, the multifactor orthogonal test was carried out according to the test factor level coding table, and the specific experimental design scheme and results are shown in Table 3.

Table 3. Test protocol and results.

Test Number	Experimental Factors			Exploratory Indicators/%	
	X_1	X_2	X_3	Y_1/N	Y_2/%
1	−1	−1	0	1083	7.18
2	1	−1	0	1120	9.88
3	−1	1	0	1103	9.31
4	1	1	0	1138	9.95
5	−1	0	−1	1102	7.89
6	1	0	−1	1131	9.18
7	−1	0	1	1095	7.21
8	1	0	1	1115	9.07
9	0	−1	−1	1186	8.11
10	0	1	−1	1181	8.47
11	0	−1	1	1156	7.59
12	0	1	1	1193	8.02
13	0	0	0	1151	8.23
14	0	0	0	1162	8.14
15	0	0	0	1154	8.37
16	0	0	0	1157	8.42
17	0	0	0	1168	8.17

(1) Establishment and test of the regression model

The test results were analyzed by Design Export 6.0.10 software, and the horizontal operating resistance Y_1 and the coefficient of variation Y_2 of the stability of the field ridge were obtained as the response function, and the horizontal coded values of each factor were the quadratic regression model of the independent variables:

$$\begin{aligned} Y_1 &= 1158.40 + 15.12X_1 + 8.75X_2 - 5.13X_3 - 57.82{X_1}^2 \\ &+10.43{X_2}^2 + 10.17{X_3}^2 - 0.50X_1X_2 - 2.2X_1X_3 + 10.50X_2X_3 \end{aligned} \tag{3}$$

$$\begin{aligned} Y_2 &= 8.27 + 0.81X_1 + 0.37X_2 - 0.22X_3 + 0.55{X_1}^2 \\ &+0.26{X_2}^2 - 0.48{X_3}^2 - 0.52X_1X_2 + 0.14X_1X_3 + 0.017X_2X_3 \end{aligned} \tag{4}$$

where Y_1 is the horizontal working resistance, N; Y_2 is the coefficient of variation of the stability of the field ridge, %; X_1 is the soil moisture content, %; X_2 is the forward speed, km·h^{-1}; X_3 is the rotation speed of the compacting device, rpm.

(2) Analysis of variance of regression equations

The obtained test data were analyzed, and the variance analysis of the horizontal operation resistance and the coefficient of variation of the stability of the firmness of the field ridge was carried out via three factors: soil moisture content, the forward speed of ridge machinery, and the rotation speed of the compacting device. The results are shown in Tables 4 and 5. As can be seen from Table 4, all factors have an impact on the horizontal operation resistance ($p < 0.01$), which shows that the regression model is extremely significant; the lack of fit had no significant effect on the horizontal operation resistance ($p > 0.05$), which shows that the quadratic regression equation fitted by the model correctly reflects the relationship between the horizontal operation resistance Y_1 and X_1, X_2, and X_3, and the regression models can make good predictions about experimental results. Among them, the primary terms X_1 (soil moisture content) and X_2 (forward speed of the ridge machinery) of the model had significant effects on the horizontal operation resistance, and X_3 (rotation speed) had a significant effect on the horizontal operation resistance; the interaction terms X_1X_2 and X_1X_3 of the model have a significant effect on the horizontal operating resistance, and X_2X_3 has an effect on the horizontal operation resistance; the quadratic term $X_3{}^2$ of the model had a significant effect on the horizontal operation resistance, while $X_1{}^2$ and $X_2{}^2$ had no significant effect on the horizontal operation resistance.

Table 4. Analysis of variance of quadratic polynomial models of horizontal operating resistance.

Source of Variance	Quadratic Sum	DOF	Mean Square	Value (*p*)
Model	17,664.81	9	1962.76	<0.0001 **
X_1	1830.12	1	1830.12	0.0002 **
X_2	612.50	1	612.50	0.0046 **
X_3	210.13	1	210.13	0.0473 *
X_1X_2	14,078.87	1	14,078.87	<0.0001 **
X_1X_3	457.60	1	457.60	0.0094 **
X_2X_3	435.92	1	435.92	0.0106 *
$X_1{}^2$	1.00	1	1.00	0.8731
$X_2{}^2$	20.25	1	20.25	0.4802
$X_3{}^2$	441.00	1	441.00	0.0103 *
Residuals	254.95	7	36.42	
Lack of fit	73.75	3	24.58	0.6786
Pure error	181.20	4	45.30	
Sum	17,919.76	16		

Note: ** indicates that the item is very significant ($p < 0.01$); * indicates that the item is significant ($p < 0.05$).

Table 5. Analysis of variance of quadratic polynomial models with the coefficient of variation of the stability of the firmness of the ridge.

Source of Variance	Quadratic Sum	DOF	Mean Square	Value (*p*)
Model	10.36	9	1.15	0.0002 **
X_1	5.27	1	5.27	<0.0001 **
X_2	1.12	1	1.12	0.0016 **
X_3	0.39	1	0.39	0.0224 *
X_1X_2	1.28	1	1.28	0.0011 **
X_1X_3	0.29	1	0.29	0.0397 *
X_2X_3	0.97	1	0.97	0.0024 **
$X_1{}^2$	1.06	1	1.06	0.0019 **
$X_2{}^2$	0.081	1	0.081	0.2230
$X_3{}^2$	1.225×10^{-3}	1	1.225×10^{-3}	0.8742
Residuals	0.32	7	0.045	
Lack of fit	0.26	3	0.086	0.0642
Pure error	0.061	4	0.015	
Sum	10.67	16		

Note: ** indicates that the item is very significant ($p < 0.01$); * indicates that the item is significant. ($p < 0.05$).

As can be seen from Table 5, all factors have an impact on the coefficient of variation of the stability of the firmness of the ridge($p < 0.01$), which shows that the regression model is extremely significant; the lack of fit had no significant effect on the horizontal operation resistance($p > 0.05$), which shows that the quadratic regression equation fitted by the model is consistent with the numerical simulation test results of the compacting device, and the relationship between the coefficient of variation Y_2 and X_1, X_2 and X_3 can be correctly reflected. The regression model can better predict the results of various experiments in the optimization experiment. Among them, the primary terms X_1 (soil moisture content) and X_2 (forward speed of the ridge machinery) of the model had significant effects on the coefficient of variation, and X_3 (working speed) had an effect on the coefficient of variation; the interaction terms X_1X_2 and X_2X_3 of the model had significant effects on the coefficient of variation, and X_1X_3 had an effect on the coefficient of variation; the quadratic term $X_1{}^2$ of the model had a significant effect on the coefficient of variation, while $X_3{}^2$ and $X_2{}^2$ had no significant effect on the coefficient of variation.

The response surface diagram of the three factors of soil moisture content (the forward speed of the machinery and the rotation speed of the compacting device to the horizontal operation resistance and the coefficient of variation of the firmness of the field ridge) is shown in Figures 6 and 7. Under the premise that the soil moisture content is certain, the horizontal operation resistance of the compacting device increases with increases in the forward speed of the ridge machinery, and the horizontal operation resistance of the compacting device first increases and then decreases with the increase in soil moisture content when the forward speed is constant, so the influence of soil moisture content on the horizontal operation resistance of the compacting device is significantly greater than that of the machinery (Figure 6a). When the forward speed of the machinery is constant, the horizontal operation resistance of the compacting device tends to have a linear relationship with the rotation speed, and the horizontal operation resistance increases with the increase in rotation speed; when the rotation speed of the compacting device is constant, the horizontal operation resistance of the compacting device increases with the forward speed of the machinery, so the influence of the forward speed of the machinery on the horizontal operation resistance of the compacting device is significantly greater than the rotation speed of the compacting device (Figure 6b). Under the premise of a certain soil moisture content, with the increasing compacting device rotation speed, the horizontal operation resistance of the compacting device gradually decreases, and the two have a linear relationship. When the rotation speed of the compacting device is constant, the horizontal operation resistance of the compacting device first increases and then decreases with an increase in soil moisture content, and when the soil moisture content changes, the horizontal operation resistance of the compacting device changes in a larger range, so the soil moisture content has a more significant effect on horizontal operation resistance (Figure 6c). By exploring the influence of the interaction between the three factors on the horizontal operation resistance of the compacting device, the degree of operation change with resistance can be predicted during the compaction. When combined with the size of the regression coefficient, it can be seen that the primary and secondary orders of the influence of each factor on the horizontal operation resistance are X_1, X_2, and X_3, which are soil moisture content, the forward speed of ridge machinery, and rotation speed of the compacting device, respectively.

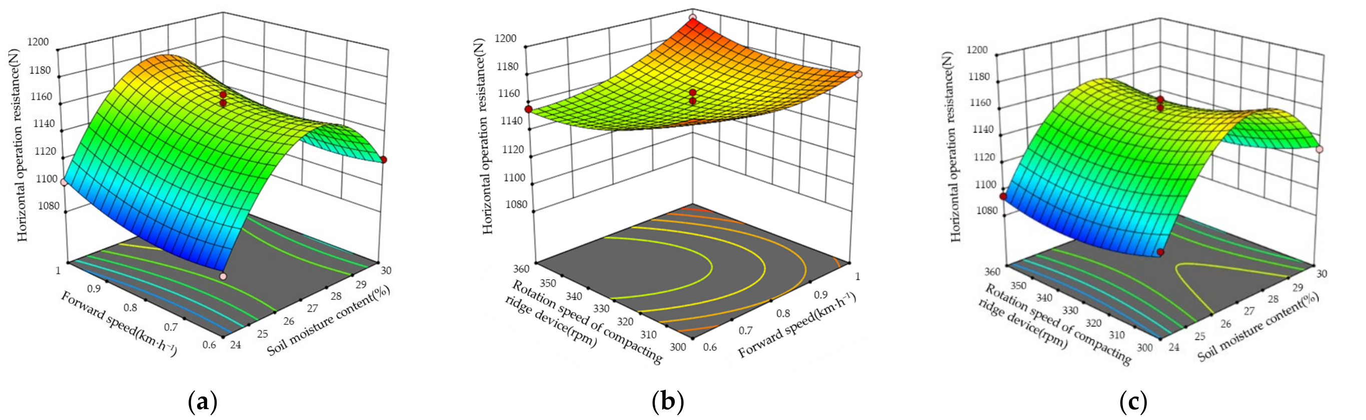

Figure 6. The response surface of each factor in accordance with horizontal operating resistance is as follows: (**a**) the forward speed and soil moisture content; (**b**) the forward speed and rotation speed; (**c**) the soil moisture content and rotation speed.

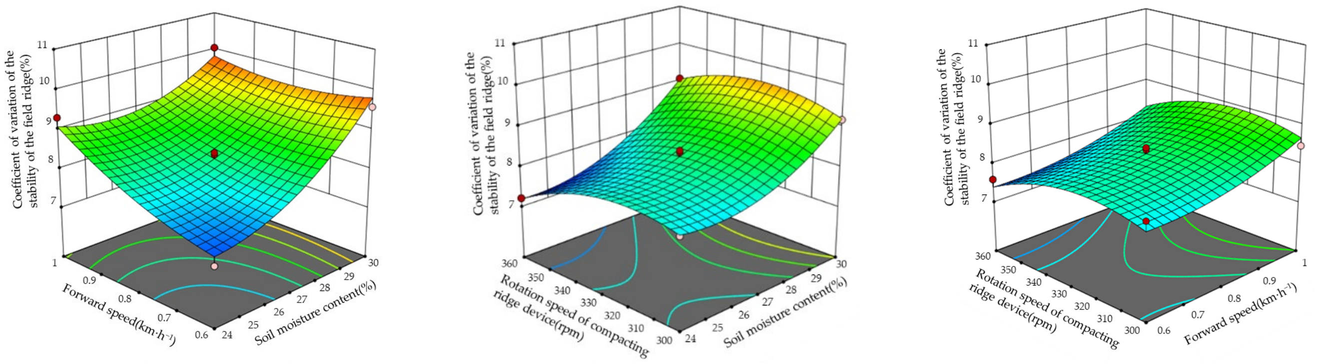

(**a**) (**b**) (**c**)

Figure 7. The response surface of each factor in accordance with the coefficient of variation is as follows: (**a**) the forward speed and soil moisture content; (**b**) the forward speed and rotation speed; (**c**) the soil moisture content and rotation speed.

Under the premise of a certain soil moisture content, with increasing forward speed (of the machinery), the coefficient of variation of the stability of the firmness of the ridge gradually increases, and the coefficient of variation gradually increases with the increase in soil moisture content when the forward speed is constant; the two have a linear relationship, so the influence of soil moisture content on the coefficient of variation is significantly greater than that of the forward speed of the machinery (Figure 7a). Under the premise of a certain soil moisture content, with increasing compacting device rotation speed, the coefficient of variation first increases and then decreases. When the rotation speed of the compacting device is constant, the coefficient of variation gradually increases with the increase in soil moisture content, and the coefficient of variation has a large range, so the influence of soil moisture content on the coefficient of variation is more significant (Figure 7b). When the forward speed of the machinery is constant, the coefficient of variation first increases and then decreases with the increase in rotation speed. When the rotation speed of the compacting device is constant, the coefficient of variation is increased by the forward speed of the machinery, and the two have a linear relationship, so the influence of the forward speed of the machinery on the coefficient of variation is more significant than that of the rotation speed of the compacting device (Figure 7c). By exploring the influence of the interaction between the three factors on the coefficient of variation, the degree of firmness change of the ridge during the compaction can be predicted. When combined with the size of the regression coefficient of each factor in the model, the main and secondary orders of influence of each factor on the coefficient of variation are X_1, X_2, and X_3: soil moisture content, the forward speed of ridge machinery, and rotation speed of the compacting device, respectively.

According to Equations (3) and (4), the horizontal operation resistance and the stability of the firmness of the ridge are the goals to ensure that the compacting device carries out the operation in the field with the lowest resistance and a dense and uniform field ridge will be formed. The experimental results show that the performance of the ridge, the quality of the operation, and the stability of the compacting device are best when the soil moisture content is 24%, the operating speed of the compacting device is 360 rpm, and the forward speed is 0.6 km·h^{-1}. The horizontal operation resistance of the compacting device is 1083.43 N, and the coefficient of variation of the stability of the firmness of the ridge is 6.52%.

(3) Analysis of the stability of the ridge firmness

Since ADAMS software can only obtain the total contact force of the ridge soil, in order to evaluate the quality of the field ridged by rotary cutting soil collection components and the compacting device, it is necessary to convert the contact force between the soil-engaging components and the ridge soil into the index of the firmness of the ridge (when combined with the bench test, the data fitting curves between the manually measured the firmness of the ridge a_1, a_2, a_3 and the uniform compacting pressure s_1, s_2, s_3) (Figure 8).

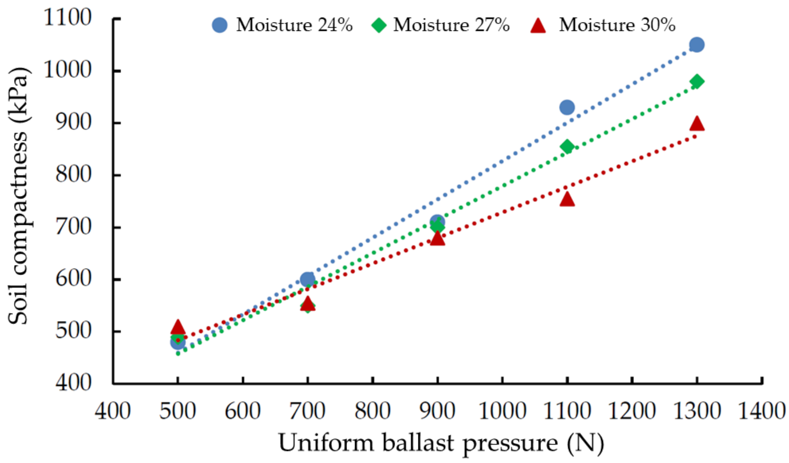

Figure 8. Relationship curve between compacting stress and firmness under different moisture content.

Under the same moisture content, the firmness of the soil increased with the increase in compacting stress and showed a linear relationship. When the uniform compacting stress exceeds 600 N, the moisture content is lower, and the firmness of the soil measured gradually increases with the increase in uniform compacting stress. The curve of the overall compacting stress of the ridge was extracted in the postprocessing module of the ADAMS software. According to the corresponding soil moisture content, it can be seen from the calculation results of Equation (2) that the forward speed of the machinery is 0.8 km·h^{-1}, the maximum and minimum firmness of the ridge are 1233.21 kPa and 953.85 kPa, respectively, and the coefficient of variation is 8.04% under the condition of moisture content of 27% (Figure 8).

3.2. Experimental Results of the Kinetic Bench Test

3.2.1. Analysis of the Soil Force for the Pinnae

The strain curve obtained by the test was analyzed (plastic deformation of the pinnae can be ignored) (Figure 9). When the forward speed of the soil tanker is 0.8 km·h^{-1}, the rotation speed of the compacting device is 320 rpm, and the sampling time is 2.5–5 s; the strain curve of the (No. 1–5) pinnae was obtained. During the operation of the compacting ridge device, with each rotation, the superimposed pinnae come into contact with the soil one after another, which causes the force of each pinna to increase from zero to maximum and gradually decreases to zero, so the counterforce of the soil only exists in the stage time during the contact between the pinnae and the soil. The analysis shows that the superimposed pinnae will successively contact the soil during each rotation of the compacting device, and the strain will change at the moment of contact between the pinnae and the soil, which causes the force of the soil on the pinnae to increase from zero to maximum and gradually decreases to zero. Therefore, the force only exists during the stage time when the pinnae are in contact with the soil.

A single (No. 5) pinna was analyzed (Figure 9b). Due to the different forces of each stage, the strain value varied greatly, with 0.5 s corresponding to a complete cycle; the reasons for the fluctuation of the strain value in a cycle and the actual significance of the strain curve were analyzed; the pinna is not in contact with the soil in the first 0.2 s, so it fluctuates around a stable value; the pinna instantly contacts the soil in the last 0.3 s, and the strain value gradually becomes larger with the increase in the contact area.

The previous pinna does not completely detach from the soil when the latter pinna begins to contact the soil, so a certain disturbance of the force is generated between the adjacent pinnae, and the peak of the force experiences an instantaneous jump phase when the adjacent pinnae contact the soil. The strain is generated when the pinnae enter the soil at the deepest level and the contact area is the largest, and the change in the strain of the pinnae exiting the soil is exactly the opposite of the process of entering the soil. The obtained strain value is converted into the force of the soil on the pinnae; the force on the pinnae is largest when the contact area with the soil is the largest and the pinnae enter the soil at the deepest level. Therefore, it cannot be ignored within the theoretical analysis of structural design and kinetic characteristics.

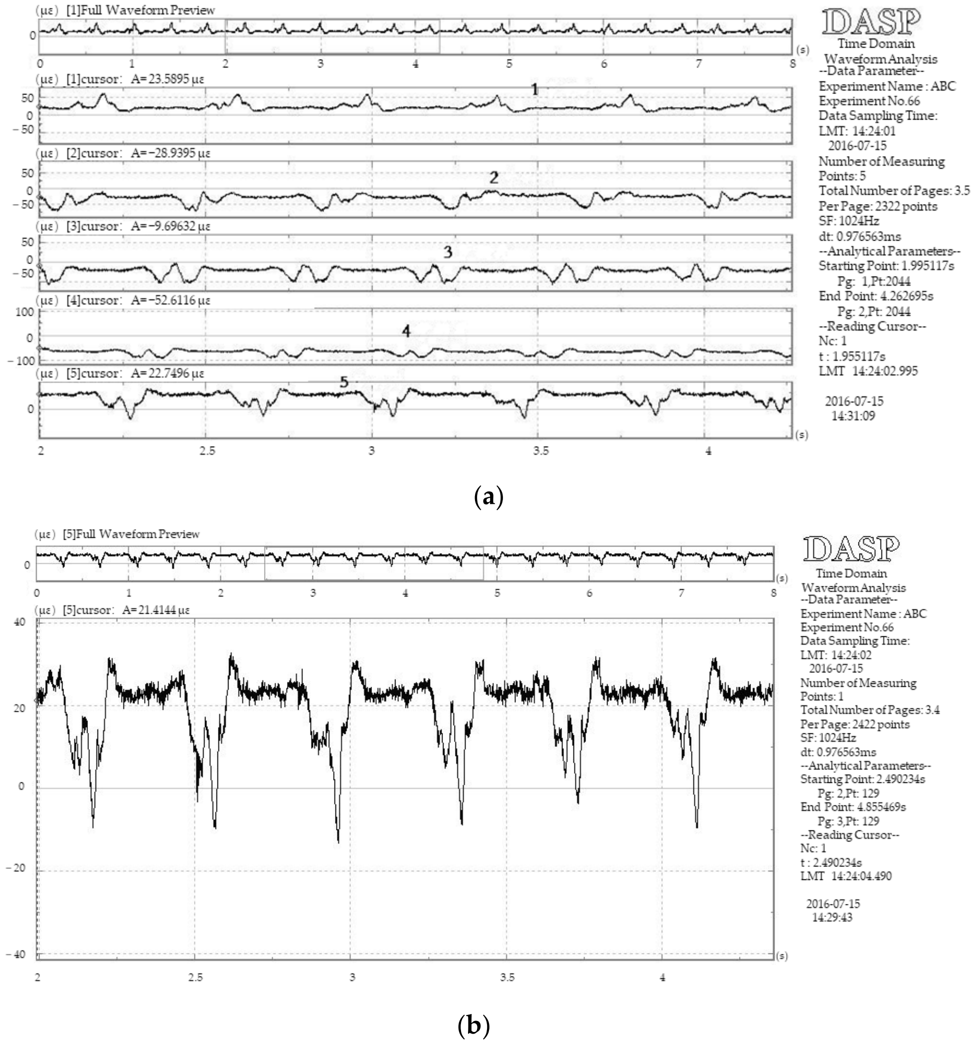

Figure 9. Test results of pinnae subjected to the soil force of the compacting device and their selfspectral analysis diagram: (**a**) curve of strain test of No. 1–5 pinnae; (**b**) curve and selfspectral analysis of strain test of No. 5 pinna.

At the same time, the selfspectral analysis plot of the pinnae with a frequency in the range of 0–512 HZ was obtained, and through the spectral analysis of a signal, it was concluded that the frequency has a high peak at 0 HZ, indicating that the random process of the force is a Gaussian random (normal random) process, and its effective value is 8.46 $\mu\varepsilon$.

3.2.2. Analysis of Ridge Firmness

The single-factor experiment was carried out by taking the forward speed of the soil tanker truck and the rotation speed of the compacting device as the influencing factors of the experiment, and the Design Export 6.0.10 software was used for data processing and analysis; the relationship between the force of the soil on the pinnae and the firmness of the ridge during the ridge operation was obtained, and the corresponding regression equation was obtained.

(1) The effect of the forward speed on the force of the pinnae and ridge firmness.

Taking the forward speed as the independent variable, the average force of the soil on the pinnae and the firmness of the ridge as the response index, the experimental results obtained are shown in Table 6.

Table 6. The average value of soil force on the pinnae and field firmness under different forward speeds.

Forward Speed/km·h^{-1}	Order			Average/N	Field Firmness/kPa
	1	2	3		
0.4	3246.70	3015.50	2252.10	2838.10	2250
0.6	5467.70	3765.50	2653.70	3962.30	2040
0.8	6954.80	3799.12	4645.40	4799.70	1930
1.0	5360.50	4996.30	5284.40	5213.70	1790
1.2	5536.20	6287.60	5261.80	5695.20	1680

Note: the rotation speed of the compacting device is 320 rpm, and the depth of the soil cutter is 180 mm.

The results of the experiment show that when the rotation speed of the compacting device and the depth of the soil cutter (into the soil) are respectively 320 rpm and 180 mm, the curve of the force of the soil on the pinnae of the compacting device is obtained, as shown in Figure 10. The average force increases and the firmness value of the ridge decreases with an increase in the forward speed of the soil tanker. When the forward speed was 0.8–1.2 km·h^{-1}, the trend of increasing average force and decreasing firmness (of the ridge) was slower than that when the forward speed was 0.4–0.8 km·h^{-1}. The regression equation for the change in force with the forward speed of the soil tanker truck is

$$y_1 = -3051{x_1}^2 + 8365x_1 + 6.67 \quad \left(R^2 = 0.996\right) \tag{5}$$

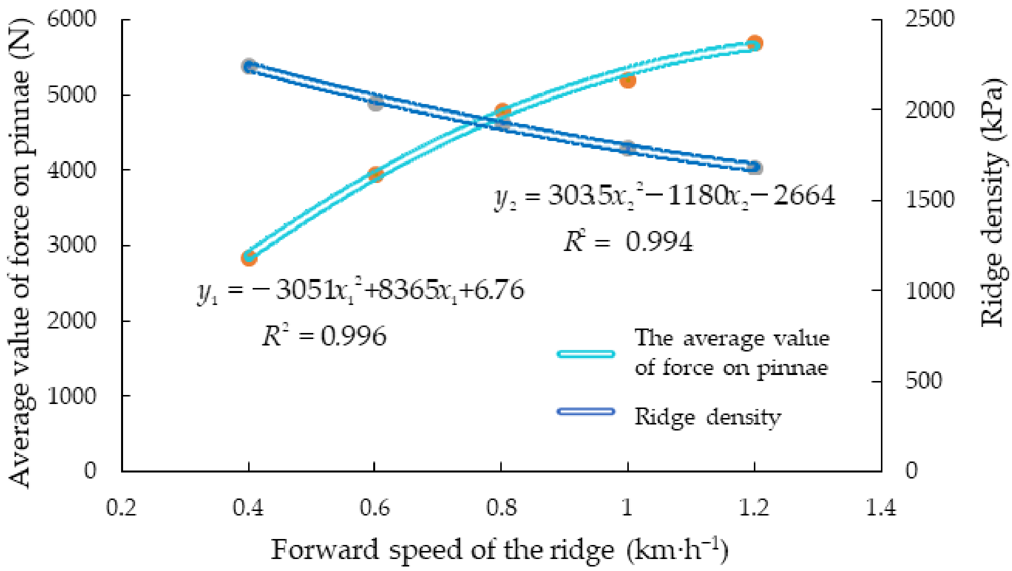

Figure 10. Curve of soil forces on the pinnae.

The regression equation for the change in the firmness value of the ridge with the forward speed of the soil tanker truck is:

$$y_2 = 303.5{x_2}^2 - 1180x_2 - 2664 \quad \left(R^2 = 0.994\right) \tag{6}$$

That is, when the forward speed of the machinery changes, the force of the soil on the pinnae increases with an increase in forward speed, and the firmness of the ridge decreases with an increase in the forward speed.

(2) The effect of the rotation speed of the compacting device on the force of the pinnae and the ridge firmness.

Taking the horizontal coding value of the speed of the compacting device as the independent variable, the average force of the pinnae, and the firmness of the ridge as the response index, the experimental results obtained are shown in Table 7.

Table 7. The average value of the soil force on the pinnae and the firmness value of the ridge under different rotation speeds of the compacting device.

Rotation Speed of Compacting Device/rpm	Order			Average/N	Field Firmness/kPa
	1	2	3		
280	2937.09	3898.70	2775.60	3203.80	1460
300	4047.50	4325.90	4383.60	4252.30	1620
320	4844.00	5271.10	4528.60	4881.20	1830
340	4867.60	5071.10	5761.70	5233.50	2060
360	6049.60	6071.25	5849.90	5990.30	2180

Note: the forward speed of the machinery is 0.8 km·h^{-1}, and the depth of the soil cutter is 180 mm.

The experimental results show that when the forward speed of the machinery and the depth of the soil cutter were, respectively, 0.8 km·h^{-1} and 180 mm, the curve of the force of the soil on the pinnae of the compacting device was formed (Figure 11). The force of the pinnae and the firmness of the ridge both increase with an increase in the rotation speed of the compacting device, and the return equation of the force with the change in the rotation speed of the compacting device is

$$y_3 = -0.153{x_3}^2 + 131.0x_3 - 21377\left(R^2 = 0.983\right) \quad (7)$$

$$y_4 = -0.010{x_4}^2 + 16.25x_4 - 2266\left(R^2 = 0.992\right) \quad (8)$$

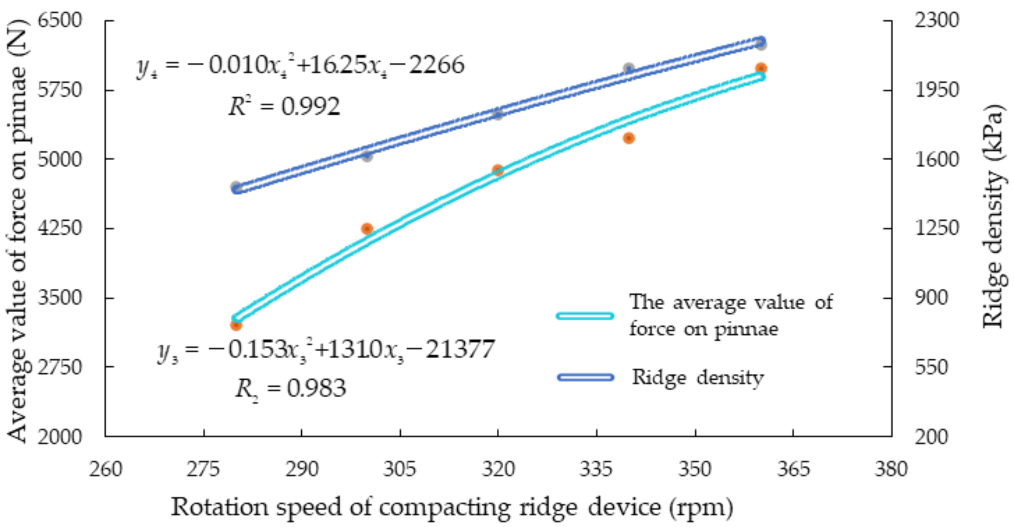

Figure 11. Curve of the firmness of the field.

That is, when the rotation speed of the compacting device changed, the force of the pinnae and the firmness of the ridge increased with an increase in rotation speed.

In summary, by using the kinetic parameter test system of the designed rotary soil-engaging components to measure the kinetic parameters of the compacting device (and analyzing the output curve), the variation law of the force of the soil on the pinnae of the compacting device was obtained, and the force is reflected in the firmness of the ridge with the difference in the forward speed and the rotation speed of the compacting device. The analysis of test data shows that, with an increase in forward speed, the number of vibrations and patting of the superimposed pinnae on the ridge per unit distance decreases when the rotation speed of the compacting device is constant, and the firmness value of the ridge is small. During the operation of the machinery, the force of the pinnae gradually increases. When the forward speed is constant, an increase in the rotation speed of the compacting device sees the number of vibrations and patting of the superimposed pinnae on the ridge per unit distance increase the firmness value of the ridge increase, and the force of soil on the pinnae also increase, correspondingly.

4. Discussion

This study takes the kinetic parameters of the rotary soil-engaging components as the research carrier, combining finite element simulation technology with bench test verification methods to explore the variation law of the acting force of soil on the pinna, the firmness of the ridge, and the influencing factors under various conditions, obtaining an optimal parameter combination. The applicability and reliability of the kinetic testing system were verified, providing a theoretical basis and data support for the measurement of the operating kinetic parameters of other rotary soil-engaging components, material selections, subsequent bench test verifications, and system developments. However, in the actual operation process, the data obtained from the kinetic testing system were also related to the soil's physical properties (firmness, density, moisture content, etc.), forward speed, roller rotation speed, tillage depth, cutting pitch, roller arrangement, cutting tool type, etc. This study did not extensively compare the relevant parameters of various rotary soil-engaging components. In subsequent research, various complex rotary soil-engaging components will be thoroughly studied while also taking into account the main agronomic indicators for ridge construction. In addition, the stress applied by the pinnae to the soil causes deformation, which is a combination of elastic and plastic processes. In order to further refine the study of this process, subsequent research will consider coupling and calibration with fluid kinetic models in order to more accurately simulate the kinetic behavior of unsaturated soil compression.

This study also designed a kinetic testing system for the ridge compacting device, using sensor testing technology to transmit signals from the pinnae through the slip ring, strain gauge, and other components to the computer. By using a combined theoretical and experimental approach, the strain curve of the pinna under the action of soil force during the construction of the ridge can be obtained. After analyzing the obtained curve, it was found that the force process of the pinna of the compacting device is a random response process. When compared with the conventional dynamic testing methods at the current stage [27], the dynamic testing system in this study has the advantages of accuracy, convenience, and relatively stable data. However, it is also characterized by high cost and can only be used for specific tillage components. Therefore, further improvements are needed for the testing system and more equipment combinations for experimentation in subsequent research.

5. Conclusions

This study focuses on the design of a kinetic system for soil-engaging components in agricultural machinery by using a compacting device for paddy field ridges as the research carrier to establish a kinetic model of the compaction process of the combined roller and pinna assembly compacting the soil during the compaction process, analyzing the operating resistance of the combined roller and pinna assembly during the compaction process. By combining numerical simulation technology and multifactor experimental methods, the ADAMS virtual simulation test and bench test were used to verify the applicability and feasibility of the system, laying an important foundation for subsequently integrated configurations of the whole machine and field tests. The following conclusions were obtained:

(1) By taking the black soil in the rice-growing area of Northeast China as the research object, a mechanical component-soil interaction model was established based on the finite element method. The compacting performance virtual test was conducted using ADAMS, and the experimental situation under different soil moisture contents was analyzed. The results showed that when the soil moisture content was 27%, the best working effect was achieved when the forward speed of the machine was 0.8 km/h and the rotation speed of the pinna-stacking compacting device was 330 r/min. The coefficient of variation of the stability of the firmness of the ridge was 8.04%;

(2) The optimal operating parameter combination of the pinna-stacking compacting device under different soil moisture conditions was studied using a three-factor and three-level experimental design. A mathematical model was established between the ridge performance indicators (horizontal operating resistance and the coefficient of variation of the stability of the firmness of the ridge) and experimental parameters (soil moisture content, forward speed, and operating rotation speed). The Design-Expert 6.0.10 software was used to analyze the experimental results and optimize the mathematical regression model. The experimental results showed that when the soil moisture content was 24%, the operating rotation speed of the pinna-stacking compacting device was 360 r/min, and when the forward speed was 0.6 km/h, the ridge performance of the pinna-stacking compacting device was optimal in terms of quality and stability, and the coefficient of variation of the stability of the firmness of ridge was 6.52%;

(3) This study proposes the design of a new type of kinetic testing system to investigate the forces acting on pinnae when the ridge compacting device interacts with the soil, measuring the related parameters. The system includes a kinetic testing system for the operating parameters of a compaction device, with the pinnae attached with strain gauges pasted onto the compacting device and connected to the kinetic testing system for real-time data acquisition. These parameters provide a theoretical basis for optimizing the structural parameters and material selection of subsequent rotary soil-engaging components.

Author Contributions: Conceptualization, J.W. (Jinwu Wang); methodology, H.T.; Y.X. and C.X.; software, Y.X.; validation, Y.X.; formal analysis, Y.X.; investigation, Y.X. and C.W.; resources, J.W. (Jinwu Wang), J.W. (Jinfeng Wang) and H.T.; data curation, Y.X. and C.W.; writing—original draft preparation, Y.X.; writing—review and editing, C.W., Z.G. and G.Z.; visualization, Y.X.; project administration, J.W. (Jinwu Wang), J.W. (Jinfeng Wang) and H.T.; funding acquisition, J.W. (Jinwu Wang). All authors have read and agreed to the published version of the manuscript.

Funding: This work was supported by the Program on Industrial Technology System of National Rice (CN), grant number: CARS-01-48.

Institutional Review Board Statement: Not applicable.

Informed Consent Statement: Not applicable.

Data Availability Statement: All data are presented in this article in the form of figures and tables.

Acknowledgments: We thank Wuxiong Weng and Nannan Lin for their contributions to the software application.

Conflicts of Interest: The authors declare no conflict of interest.

References

1. Liu, L.; Wang, L.J.; Hu, H. Research Status and Application of Bionic Adhesive Reduction Technology for Soil Touching Parts of Agricultural Machinery. *Agric. Equip. Veh. Eng.* **2022**, *60*, 27–31. [CrossRef]
2. Matin, M.A.; Fielke, J.M.; Desbiolles, J.M.A. Torque and Energy Characteristics for Strip-Tillage Cultivation When Cutting Furrows Using Three Designs of Rotary Blade. *Biosyst. Eng.* **2015**, *129*, 329–340. [CrossRef]

3. Matin, M.A.; Desbiolles, J.M.A.; Fielke, J.M. Strip-Tillage Using Rotating Straight Blades: Effect of Cutting Edge Geometry on Furrow Parameters. *Soil Tillage Res.* **2016**, *155*, 271–279. [CrossRef]
4. Ahmadi, I. A Torque Calculator for Rotary Tiller Using the Laws of Classical Mechanics. *Soil Tillage Res.* **2017**, *165*, 137–143. [CrossRef]
5. Ucgul, M.; Saunders, C.; Li, P.; Lee, S.-H.; Desbiolles, J.M.A. Analyzing the Mixing Performance of a Rotary Spader Using Digital Image Processing and Discrete Element Modelling (DEM). *Comput. Electron. Agric.* **2018**, *151*, 1–10. [CrossRef]
6. Tong, J.; Ji, W.; Jia, H.; Chen, D.; Yang, X. Design and Tests of Biomimetic Blades for Soil-Rototilling and Stubble-Breaking. *J. Bionic Eng.* **2015**, *12*, 495–503. [CrossRef]
7. Wang, L.J.; Liao, J.Y.; Hu, H. Research Status and the Prospect of Adhesion Reduction and Desorption Technology for Agricultural Machinery Parts Touching Soil. *J. Chin. Agric. Mech.* **2021**, *42*, 214–221. [CrossRef]
8. Ma, W.P.; You, Y.; Wang, D.C. Design and Experiment of Low-Resistance Soil Loosening Shovel for Cutting Roots and Reseeding in Perennial Alfalfa Field. *Trans. Chin. Soc. Agric. Mach.* **2021**, *52*, 82–95. [CrossRef]
9. Zhang, Z.H.; Zhao, L.L.; Lai, Q.H. Operation Mechanism Analysis and Experiments of Shovel-Type Rolling Soil-Engaging Components Based on DEM-MBD Coupling. *Trans. Chin. Soc. Agric. Eng.* **2022**, *38*, 10–20.
10. Salem, A.E.; Wang, H.C.; Gao, Y.; Zha, X.T. Effect of Biomimetic Surface Geometry, Soil Texture, and Soil Moisture Content on the Drag Force of Soil-Touching Parts. *Appl. Sci.* **2021**, *11*, 8927. [CrossRef]
11. Zhang, Y.P.; Du, R.C.; Diao, P.S. Experiment of No-Tillage and Drought Direct Sowing Rice and Feasibility Analysis in Shangdong Province. *Trans. Chin. Soc. Agric. Eng. Trans. CSAE* **2016**, *32*, 24–30.
12. Li, H.L.; Liu, G.; Chen, M.C. Discussion on the Technique of Rice Production Mechanization in China. *Agric. Sci. Technol. Equip.* **2014**, *12*, 38–39. [CrossRef]
13. Zuo, X.J.; Wu, G.W.; Fu, W.Q. Design and Experiment on Air-Blast Rice Side Deep Precision Fertilization Device. *Trans. Chin. Soc. Agric. Eng. Trans. CSAE* **2016**, *32*, 21–41.
14. Liu, M.Y.; Ku, H.F.; Cai, H. Optimization Design and Analysis of the Blade Laminated Ridger for Paddy Field. *J. Chin. Agric. Mech.* **2019**, *40*, 31–36.
15. Zhao, Y. Mechanism Analysis and Design of Ridger for Paddy Fields. *Harbin Northeast Agric. Univ.* **2015**.
16. Wang, J.F.; Lin, N.N.; Wang, J.W. Design and Experiment on Working Dynamics Parameters of Single-Side Ridger. *Trans. Chin. Soc. Agric. Mach.* **2017**, *48*, 81–86+104. [CrossRef]
17. Wang, J.F.; Wang, J.W.; Kong, Y.J. Development and Experiment of Suspension Ridger and Its Key Components for Paddy Field. *Trans. Chin. Soc. Agric. Eng. Trans. CSAE* **2013**, *29*, 28–34. [CrossRef]
18. Yang, Y.S.; Ding, Q.S.; Ding, W.M. Design and Application of Multi Purpose in Situ Tillage Tool Testing Platform. *Trans. Chin. Soc. Agric. Mach.* **2016**, *47*, 68–74.
19. Wang, J.W.; Tang, H.; Wang, J.F. Design and Experiment on 1DSZ-350 Type Hanging Unilateral Rotary Tillage Compacting Ridger for Paddy Field. *Trans. Chin. Soc. Agric. Eng.* **2017**, *33*, 25–37.
20. Azimi-Nejadian, H.; Karparvarfard, S.H.; Naderi-Boldaj, M. Combined Finite Element and Statistical Models for Predicting Force Components on a Cylindrical Mouldboard Plough. *Biosyst. Eng.* **2019**, *186*, 168–181. [CrossRef]
21. Wang, X.J.; Song, J.N.; Liu, C.L. Design and Experiment on Licorice Tilt Transplanting Furrow Opener. *Trans. Chin. Soc. Agric. Eng. Trans. CSAE* **2016**, *32*, 16–23.
22. Zhang, J.X.; Cai, W.; Tan, F. Design and Analysis of ADAMS Simulation for a New-Type Automobile Steering Mechanism. *Adv. Mater. Res.* **2013**, *706–708*, 1250–1253. [CrossRef]
23. Gamaniel, S.S.; Dini, D.; Biancofiore, L. The Effect of Fluid Viscoelasticity in Lubricated Contacts in the Presence of Cavitation. *Tribol. Int.* **2021**, *160*, 107011. [CrossRef]
24. Jaramillo, A.; Buscaglia, G.C. An Extended Elrod-Adams Model to Account for Backpressure and Blow-by Inception. *Tribol. Int.* **2019**, *140*, 105873. [CrossRef]
25. Lu, Z.R.; Liu, G.; Liu, J. Parameter Identification of Nonlinear Fractional-Order Systems by Enhanced Response Sensitivity Approach. *Nonlinear Dyn.* **2019**, *95*, 1495–1512. [CrossRef]
26. Wang, J.F.; Weng, W.X.; Wang, J.W. Design and Experiment of Bi-Directional Ridger for Paddy Field. *Trans. Chin. Soc. Agric. Mach.* **2019**, *50*, 40–48. [CrossRef]
27. Liu, S.T.; Xia, J.P.; Gao, X.C.; Yang, G. L. Laboratory test of kinetic parameters of compacted soil specimen. *J. Chang. Univ. Nat. Sci. Ed.* **2022**, *42*, 4. [CrossRef]